Dossier

This paper is a part of the hereunder thematic dossier published in OGST Journal, Vol. 69, No. 2, pp. 195-372 and available online here

Cet article fait partie du dossier thématique ci-dessous publié dans la revue OGST, Vol. 69, n°2, pp. 195-372 et téléchargeable ici

DOSSIER Edited by/Sous la direction de : **L. Duval**

Advances in Signal Processing and Image Analysis for Physico-Chemical, Analytical Chemistry and Chemical Sensing

Progrès en traitement des signaux et analyse des images pour les analyses physico-chimiques et la détection chimique

Oil & Gas Science and Technology – Rev. IFP Energies nouvelles, Vol. 69 (2014), No. 2, pp. 195-372

Oil & Gas Science and Technology – Rev. IFP Energies nouvelles, Vol. 69 (2014), No. 2, pp. 229-244

DOI: 10.2516/ogst/2012092

Dossier

Advances in Signal Processing and Image Analysis for Physico-Chemical, Analytical Chemistry and Chemical Sensing
Progrès en traitement des signaux et analyse des images pour les analyses physico-chimiques et la détection chimique

NMR Data Analysis: A Time-Domain Parametric Approach Using Adaptive Subband Decomposition

E.-H. Djermoune*, M. Tomczak and D. Brie

Centre de Recherche en Automatique de Nancy (CRAN), Université de Lorraine, CNRS, Bd des Aiguillettes, BP 239, 54506 Vandœuvre-lès-Nancy Cedex - France
e-mail: el-hadi.djermoune@cran.uhp-nancy.fr - marc.tomczak@cran.uhp-nancy.fr - david.brie@cran.uhp-nancy.fr

* Corresponding author

Résumé — Analyse de données RMN : une approche paramétrique basée sur une décomposition en sous-bandes adaptative — Dans ce papier, nous proposons une méthode rapide d'analyse de signaux de spectroscopie de Résonance Magnétique Nucléaire (RMN), dans le cas Lorentzien, fondée sur une décomposition adaptative en sous-bandes. Cette dernière est obtenue par une succession d'étages de filtrage/décimation aboutissant à un arbre de décomposition. À chaque noeud de l'arbre, les paramètres du signal correspondant à la sous-bande sont estimés par une méthode haute-résolution. Puis l'erreur d'estimation est utilisée dans un test d'arrêt qui permet de décider si la décomposition doit être poursuivie ou non dans cette branche. Ainsi, cette approche permet la sélection automatique du niveau de décimation ce qui conduit la décomposition à s'adapter au contenu fréquentiel du signal. De plus, la méthode entraîne une réduction du temps de calcul et facilite le choix des paramètres libres comparativement à une analyse globale du signal. Son efficacité est illustrée au travers d'exemples de signaux RMN ^{13}C 1-D et 2-D.

Abstract — NMR Data Analysis: A Time-Domain Parametric Approach Using Adaptive Subband Decomposition *— This paper presents a fast time-domain data analysis method for one- and two-dimensional Nuclear Magnetic Resonance (NMR) spectroscopy, assuming Lorentzian lineshapes, based on an adaptive spectral decomposition. The latter is achieved through successive filtering and decimation steps ending up in a decomposition tree. At each node of the tree, the parameters of the corresponding subband signal are estimated using some high-resolution method. The resulting estimation error is then processed through a stopping criterion which allows one to decide whether the decimation should be carried on or not. Thus the method leads to an automated selection of the decimation level and consequently to a signal-adaptive decomposition. Moreover, it enables one to reduce the processing time and makes the choice of usual free parameters easier, comparatively to the case where the whole signal is processed at once. The efficiency of the method is demonstrated using 1-D and 2-D ^{13}C NMR signals.*

INTRODUCTION

Since its discovery in 1945, the Nuclear Magnetic Resonance (NMR) spectroscopy has become a powerful and very successful tool to study chemical structures and molecular interactions [1]. The multidimensional NMR widens the field of investigation to the study of macromolecular structures by allowing the detection and interpretation of interactions that are impossible to analyze along a single dimension (see *e.g.* [2, 3]). This paper considers the general

problem of determining the parameters of one-dimensional (1-D) and two-dimensional (2-D) NMR signals. Theoretically, the spectra of these signals exhibit Lorentzian lineshapes (corresponding to exponentially decaying signals) ([4], pp. 69-71) but, in some cases, because of acquisition conditions, the lineshapes may be broadened [5] and thus modeled by Gaussian or Voigt shapes [6]. For example, this is often the case in ^{1}H spectroscopic data in which the deviation is due to residual eddy currents and magnetic field inhomogeneities [7]. Here, we propose an efficient methodology based on subband decomposition to deal with intricate NMR signals and we focus on Lorentzian lineshapes though our approach may be easily adapted to other model functions. Hence, the model considered here for a 1-D NMR signal is the normal one; *i.e.* the superposition of K damped exponentials (also called *modes* or *resonances*) in noise:

$$x(n) = \sum_{k=1}^{K} A_k e^{-\alpha_k n} e^{\imath(\omega_k n + \phi_k)} + e(n) = \sum_{k=1}^{K} a_k z_k^n + e(n) \quad (1)$$

for $n = 0, \ldots, N-1$. Here, $z_k = \exp(-\alpha_k + \imath\omega_k)$ is a signal mode ($\omega_k = 2\pi f_k$) and $a_k = A_k \exp(\imath\phi_k)$ is the complex amplitude, where $\alpha_k, A_k \in \mathbb{R}^+$ and $\omega_k, \phi_k \in [-\pi, +\pi]$. N is the number of samples and $\imath := \sqrt{-1}$ stands for the imaginary unit. Note that the sampling period is included in α_k and ω_k for notation simplicity. The term $e(n)$ is assumed to be complex white noise. Similarly, a 2-D NMR signal can be written as:

$$x(n,m) = \sum_{k=1}^{K} a_k z_k^n w_k^m + e(n,m) \quad (2)$$

for $n = 0, \ldots, N-1$ and $m = 0, \ldots, M-1$. In this case, $z_k = \exp(-\alpha_{1,k} + \imath\omega_{1,k})$ and $w_k = \exp(-\alpha_{2,k} + \imath\omega_{2,k})$ are the components of the mode (z_k, w_k) with amplitude $a_k = A_k \exp(\imath\phi_k)$. The parameters $\omega_{\bullet,k}$, $\alpha_{\bullet,k}$, A_k and ϕ_k are in the same ranges as before. Note that these models are common to many other applications such as sonar, radar, mobile communications and mechanical vibrations, making the proposed approach not restricted to NMR signal analysis.

The problem is to estimate the parameters K, a_k and more specifically z_k (and w_k for 2-D signals) from data samples. The classical way to obtain these parameters consists in using the Fourier Transform (FT) whose calculation is indeed simple and fast but the corresponding estimator suffers from the so-called Rayleigh resolution limit [(1)] ([8], p. 46) and presents a poor variance ([9], p. 69). Moreover, due to the frequent overlaps of nearby modes, amplitudes cannot be well estimated by simple numerical integration, and it is necessary to resort to some nonlinear optimization procedures resulting in highly time consuming algorithms along with their convergence problems [10]. Consequently, several alternative approaches have been proposed in the last 20 years. They are based on different concepts such as linear prediction, signal and noise subspace separation, maximum likelihood [11], Bayesian inference [12], etc. For damped/undamped sinusoidal signals in noise, the most used methods are those related to the concept of signal or noise subspaces, also called eigenanalysis methods. For 1-D signals, we can cite the Kumaresan and Tufts method [13], state-space methods [14] and matrix pencil [15]. These methods and their variants have been applied successfully to NMR data, often using other acronyms such as LPSVD (Linear Prediction-Singular Value Decomposition), HSVD (Hankel-Singular Value Decomposition) and so on [16-20] (see also the review paper by Poullet *et al.* [21] and the references therein for more details). Several methods have been also proposed for 2-D and multidimensional modal signals. They are often extensions of 1-D approaches, such as 2-D IQML [22], 2-D MUSIC [23], TLS-Prony [24], Matrix Enhancement and Matrix Pencil (MEMP) [25], etc. Other have been specifically developed for 2-D signals such as MultiDimensional Folding (MDF) [26], MultiDimensional Embedding (MDE) [27] and 2-D ESPRIT [28].

All these methods present several advantages over the FT in terms of resolution and detection, and what is more, most of them are non-iterative schemes able to yield directly the relevant parameters. However, at the present time, the FT still remains the standard procedure for NMR signal analysis. This is probably due to some of the drawbacks of these estimators. Firstly, all of them generally require some trial-and-error adjustment, especially concerning the choice of the number of pertinent parameters (*i.e.* the model order K). Secondly, although several criteria have been proposed for the estimation of the number of modes, *e.g.* the Minimum Description Length (MDL) [29], none are fully reliable. Thirdly, the time spent for the computation is generally much longer than that of the FT. Finally, when the signals are of high complexity, *i.e.* made up of numerous data samples (over 10 000) and/or containing a very large number of modes, all the problems are becoming much more crucial leading to a sensible degradation of the overall performance. In some situations, the problem may even become numerically untractable because of the prohibitive computation cost and memory capacities requested.

The last two aforementioned problems have motivated, last years, a renewed interest for subband-based approaches [30-34] that have been known for a long time in the signal processing community. The idea is to process a signal by splitting it into several small spectral windows. In the NMR literature, this concept has been initially proposed in 1988 by Tang and Norris with the LP-ZOOM approach [35]. The subband approach may be seen as a pre-processing of the signal, and thus is independent from the method used for the estimation. In addition to

(1) The spectral resolution of spectral estimators based on the FT is approximately equal to the reciprocal of the signal duration in the noiseless case.

their computational efficiency, these techniques present several other advantages comparatively to a fullband estimation [32, 36, 37]. In particular, it is known that data decimation (or downsampling) may increase the resolution capabilities of the estimator considered [38] and enables one to process signals at low signal-to-noise ratios [39]. Several subband methods have been proposed in the NMR literature (see *e.g.* [36, 40-45]). Recently, Sandgren *et al.* [46] proposed a survey of the main subband methods and discussed their estimation performances. All these techniques share two features that make them efficient with high-complexity signals: high robustness against out-of-band interferences and low computational burden. In practice, it is often desirable to perform an analysis of the whole spectral band. In this case, without *a priori* information, the problem remains of how to select the spectral subbands, their width and their location, or equivalently the depth of the decomposition.

One solution to the problem of choosing the depth of the decomposition is given by adaptive approaches. For example, in the best basis paradigm involving wavelet packet expansions [47-50], the idea is to select the collection of nodes that minimize a given criterion. At each node of the decomposition tree, the cost is compared with the cost of the union of its two children's nodes and if the node's cost is smaller than the children's costs, the node is retained; otherwise, the children nodes are retained instead of the node itself. For spectral analysis, most of the decompositions are based on the MDL principle [51, 52]: the decomposition is stopped if the estimated number of modes in a particular node is greater than the one obtained in its children. The problem which arises with such an approach is that it does not ensure that all the spectral information has been retrieved because the decision is taken before the subband estimation. Thus the resulting partition does not take into account the fact that an isolated mode may be estimated without needing a deeper decomposition. Here, we propose a method using another stopping rule in order to circumvent this problem. The adaptive partition is achieved through successive decimation/estimation stages each followed by a test procedure which is based on a local spectral flatness measure of the estimation residuals, in order to decide whether or not the process should continue. This criterion reflects the quality of the estimation in a given subband, so the decomposition is stopped only if the residuals are close to white noise, *i.e.* all local modes are retrieved. The resulting approach not only selects automatically the subbands where spectral peaks are present and reject the others but also allows the algorithm to stop the decomposition on the bands where all modes may be easily extracted without the need of a deeper decomposition [39]. Moreover, the measure of flatness may be easily extended for multidimensional signals.

The sequel of this paper is organized as follows. In Section 1, we present the principles of 1-D and 2-D subband decompositions and the model of the resulting signals. Then in Section 2, the adaptive approach is detailed along with the stopping rule used. Section 3 is dedicated to the implementation issues and presents the summary of the algorithms. The procedure to download the MATLAB code of the method is also given. Finally, results on 1-D and 2-D experimental NMR signals are presented in Section 4. Conclusion are drawn at the end.

1 PRINCIPLES OF SUBBAND DECOMPOSITION

1.1 1-D Signals

Subband decomposition of 1-D signals is achieved by successive filtering and downsampling stages. Frequently, the downsampling factor between two levels is 2, leading to the tree illustrated in Figure 1. Notation $x_\ell^{(i)}(n)$ stands for the subband signal at level ℓ representing the spectral band number i, where $i = 0, \ldots, 2^\ell - 1$ corresponds to a frequency shift. In other words, the original signal $x_0^{(0)}(n) := x(n)$ is split at level ℓ into 2^ℓ subband signals, each of them is representative of a specific frequency interval localized by the index i. We will be more specific on this point in Section 3.1. The decomposition of any node of the tree is

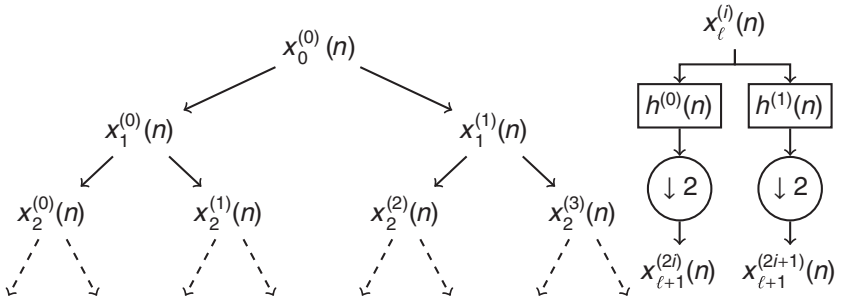

Figure 1

Principle of subband decomposition of a 1-D signal. $x_0^{(0)}(n) := x(n)$ and $h^{(i)}(n)$ are the impulse responses of complementary digital bandpass filters.

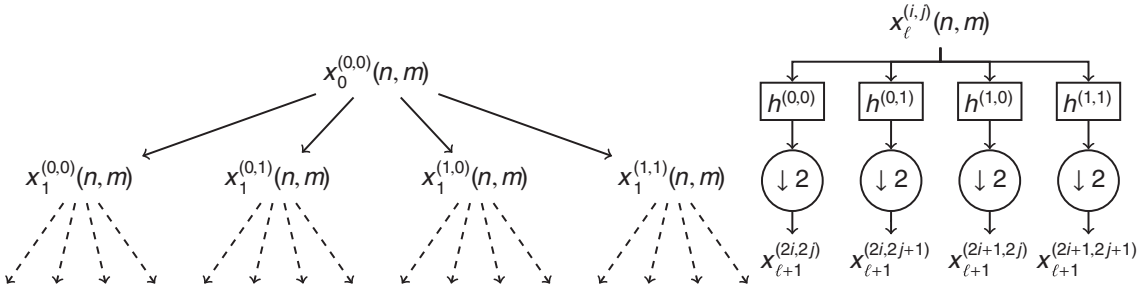

Figure 2

Principle of subband decomposition of a 2-D signal. $x_0^{(0,0)}(n,m) := x(n,m)$ and $h^{(i,j)}(n,m)$ are the impulse responses of complementary digital bandpass filters.

achieved through filtering and decimation and thus can be expressed as:

$$x_{\ell+1}^{(2i)}(n) = \sum_{n'} h^{(0)}(n') x_\ell^{(i)}(2n - n') \tag{3}$$

$$x_{\ell+1}^{(2i+1)}(n) = \sum_{n'} h^{(1)}(n') x_\ell^{(i)}(2n - n') \tag{4}$$

for $n = 0, \ldots, [N_\ell/2] - 1$, where N_ℓ is the length of signal $x_\ell^{(i)}(n)$ and $[\bullet]$ stands for the integer part function. It can be shown that the resulting signals can still be modeled as a combination of (a reduced number of) modes [32, 44]. For notation simplicity, let $x'(n)$ be a subband signal and v' be the subband image of the fullband parameter v, then the model of the subband signal is:

$$x'(n) \approx \sum_{k=1}^{K'} a'_k z'^n_k + e'(n) \tag{5}$$

Hence, the model being of the same form as in Equation (1), it is possible to use the same methods discussed before to estimate the parameters z'_k and a'_k. In practice, it is desirable to be able to convert these values to their fullband counterparts using simple formulae. This point will also be discussed in details in Section 3.1. The advantages of estimating the signal parameters from subbands are twofold. First, each subband signal is expected to contain less modes than $x(n)$ (*i.e.* $K' \leqslant K$). Second, the number of samples is also reduced because of the downsampling operation. These two features result in a much less time-consuming and numerically more tractable estimation procedure. One could think that the estimation variance should increase as the number of samples decreases but it should be recalled that the number of unknown parameters is also prone to be reduced comparatively to the fullband signal. Anyway, a maximum decimation depth must be imposed to avoid critical situations with a very few samples in the subbands, which could lead to a strong degradation of the estimation variance. One solution to this problem is presented in Section 2.

1.2 2-D Signals

Subband decomposition of 2-D signals is achieved in a multilevel way, similar to what was presented before. Here, the spectral domain is two-dimensional. Hence, four 2-D filters are necessary to achieve the decimation from level ℓ to level $\ell+1$ as illustrated in Figure 2. The decomposition of a signal $x_\ell^{(i,j)}(n,m)$ with size $N_\ell \times M_\ell$ is obtained as:

$$x_{\ell+1}^{(2i+i',2j+j')}(n,m) = \sum_{n',m'} h^{(i',j')}(n',m') x_\ell^{(i,j)}(2n - n', 2m - m') \tag{6}$$

for i' and j' in $\{0,1\}$, $n = 0, \ldots, [N_\ell/2] - 1$ and $m = 0, \ldots, [M_\ell/2] - 1$. The filters are chosen so that their passbands do not intersect. Consequently, the spectral lines in $x_\ell^{(i,j)}(n,m)$ are separated into four groups each corresponding to a subband signal. Here again, the model of the subband signals is of the same form as in fullband, *i.e.*:

$$x'(n,m) \approx \sum_{k=1}^{K'} a'_k z'^n_k w'^m_k + e'(n,m) \tag{7}$$

2 ADAPTIVE DECOMPOSITION

The subband decomposition approach was shown to have several advantages over a fullband estimation in the case of high complexity signals [53] but it still strongly depends on the right choice of the degree of decomposition. Indeed, in practice, it is necessary to fix the total decimation factor, thus the number of subbands and their sizes. This choice is depending on the signal at hand and requires some *a priori* knowledge that is generally not available. Theoretically, the smaller the size of the window, the better the overall performances (numerical complexity, resolution, estimation and detection). But since the length of the subband signals decreases with decreasing spectral window size, it is very likely that the estimation variance and detection performances will degrade themselves beyond a certain limit. Thus it is clear that an optimal degree of decomposition is existing. The idea behind an adaptive subband

decomposition is to fully exploit the multi-level of the subband decomposition by deciding at each node whether the decimation should continue or stop. This scheme allows the decomposition to adapt itself to the spectral content of the analyzed signal generally resulting in a non-uniform decomposition tree. The decision about pursuing or not the decomposition has to be made according to some criterion. For example, it is possible to test the content of either the subband signal or the estimation error. It has been observed [53] that residual-based stopping rules are preferable because they tend to minimize the number of final nodes while preserving good estimation conditions.

2.1 1-D Signals

The signal model at a given node is given in Equation (5). Let $\hat{z}'_k, \hat{a}'_k$ and $\hat{K}'$ be the parameters estimated in a given subband, for $k = 1, \ldots, \hat{K}'$. The residual signal is then defined by:

$$\varepsilon(n) = x'(n) - \hat{x}'(n) := x'(n) - \sum_{k=1}^{\hat{K}'} \hat{a}'_k \hat{z}'^{n}_k \tag{8}$$

If the modes have been correctly estimated (*i.e.* $\hat{K}' = K'$, $\hat{z}'_k \approx z'_k$ and $\hat{a}'_k \approx a'_k$), then the residual signal should be close to white noise. So the whiteness of the residual is the criterion to be used for the decomposition. A lot of spectral flatness tests have been proposed among which Fisher's whiteness test [54] is the most popular. In the case of damped complex exponentials signals, we found that Drouiche's test [55] is more appropriate because of a better detection rate [56]. The latter is based on the so-called periodogram estimate of the Power Spectral Density (PSD) of $\varepsilon(n)$ defined by:

$$\hat{P}'(\omega) = \frac{1}{N'} \left| \sum_{n=0}^{N'-1} \varepsilon(n) e^{-\imath n\omega} \right|^2 \tag{9}$$

The spectral flatness measure, restricted to the interval $[-\pi/2, \pi/2]$, is given by the following quantity [(2)] [55]:

$$\hat{W}' = \ln \frac{1}{\pi} \int_{-\frac{\pi}{2}}^{\frac{\pi}{2}} \hat{P}'(\omega) d\omega - \frac{1}{\pi} \int_{-\frac{\pi}{2}}^{\frac{\pi}{2}} \ln \hat{P}'(\omega) d\omega - \gamma \tag{10}$$

where γ is the Euler constant ($\gamma \approx 0.57721$). In order to decide whether or not $\hat{P}'(\omega)$ is flat (or constant), the quantity $\hat{W}'$ is compared to a threshold λ_α which is fixed according to the desired false alarm rate α by using the following relation:

$$\lambda_\alpha = \sqrt{\frac{2(\pi^2/6 - 1)}{N'}} \mathrm{erf}^{-1}(1 - 2\alpha) \tag{11}$$

where $\mathrm{erf}^{-1}(x)$ is the inverse of the standard error function. In this paper, it is fixed to 1%. The decision about stopping or carrying on the decomposition is then taken according to the following rule:

$$\begin{cases} \text{if } \hat{W}' < \lambda_\alpha \text{ then stop} \\ \text{if } \hat{W}' \geqslant \lambda_\alpha \text{ then continue} \end{cases} \tag{12}$$

2.2 2-D Signals

For 2-D signals, the adaptive procedure is similar except the fact that the spectral flatness is measured on the 2-D plane. Let $\varepsilon(n, m)$ be the residual signal in a given subband, then its PSD is estimated by:

$$\hat{P}'(\omega_1, \omega_2) = \frac{1}{N'M'} \left| \sum_{n=0}^{N'-1} \sum_{m=0}^{M'-1} \varepsilon(n, m) e^{-\imath n\omega_1} e^{-\imath m\omega_2} \right|^2 \tag{13}$$

Then, we may apply the previous measure in Equation (10) on the two marginals of $\hat{P}'(\omega_1, \omega_2)$ along the two dimensions to obtain $\hat{W}'_1$ and $\hat{W}'_2$. Now, the signal $\varepsilon(n, m)$ is a white noise only if the two measures are less than a threshold λ_α.

3 IMPLEMENTATION

In this section, we discuss the implementation issues of the proposed method and then we give the complete algorithms for 1-D and 2-D NMR data analysis.

3.1 The Filter Bank

Generally, the subband decomposition is achieved through wavelet packet-like filter banks [52]. Such filters are designed to ensure perfect reconstruction of the signal, which implies a slight overlapping between the two filters as illustrated in Figure 3a. In the particular case of spectral analysis in which we would estimate the spectral parameters in subband without the need of signal reconstruction, this type of filter bank is inappropriate because it causes two undesirable effects. First, the filters attenuate all peaks appearing in the vicinity of band edges (*Fig. 3a*: around normalized frequencies −0.25 and +0.25). Hence, the estimated modes lying in this spectral region will exhibit some distorsion. The second and more important effect is frequency aliasing after decimation because the effective bandwidth [(3)] of each filter is somewhat greater than 1/2. For example, if some spectral lines with strong intensities appear around the normalized frequency 0.25, they will be captured in two distinct subbands [57]. This implies that a single fullband frequency could have two distinct subband images. In other

(2) In practice, the integrals are approximated by discrete sums. Thus $\hat{P}'(\omega)$ is evaluated at the Fourier bins using the fast Fourier transform.

(3) The filter's bandwidth has several definitions including –3 dB and zero-crossing bandwidths. In this paper, it is defined as the sum of the pass- and transition band widths.

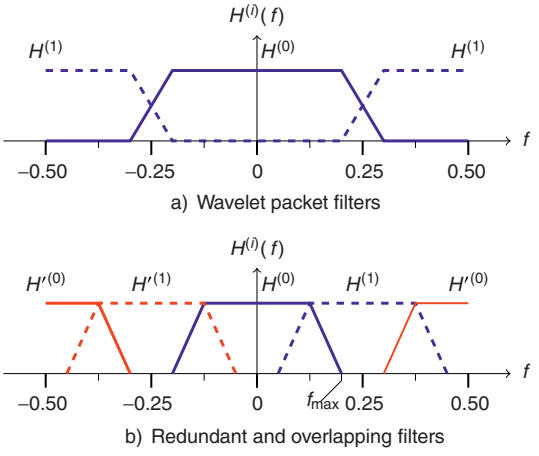

Figure 3

Frequency responses of a) wavelet packet-like and b) completely overlapping filter banks. $f_{\max}$ is the frequency delimiting the end of the transition band of the central filter.

words, the relation $z_k \mapsto z'_k$ is not a bijection and thus it will be difficult to map the subband modes to their fullband counterparts [33]. Consequently, we rather use the oversampled filter bank sketched in Figure 3b. In order to minimize aliasing due to decimation by 2, the bandwidth (including passband and transition bands) of each filter is less than or equal to $1/2$ (the attenuation in the stopband is assumed to be strong enough to eliminate all out-of-band spectral lines). As a result, the passbands of the filters are contiguous and the transition bands of two successive filters are overlapping. The simplest way to choose the adequate analysis filter bank is to set the total passband width of each filter to $1/4$, which supposes the use of 4 similar filters as illustrated by Figure 3b. Moreover, to guarantee a one-to-one correspondence between fullband and subband modes, only those estimated in the central regions (passbands) should be retained; this implies that the modes detected in the transition bands are simply discarded (if a mode appears in the transition band of a given filter, it appears necessarily in the passband of an adjacent one). Specifically, as in [31], we use 50% spectral overlap of the subbands, which allows a final retention of the central half of each of them [(4)]. Indeed, in our case, the number of necessary filters is doubled comparatively to wavelet packet.

It is important to note that it is still possible to use the classical cascade scheme illustrated in Figure 1 to perform subband decomposition based on the oversampled filter bank. As this scheme calls for only two filters, it is necessary to perform two decompositions, each being associated with half the spectral range $[-0.5, 0.5]$. Here, the frequency bands $[-0.5, 0]$ and $[0, 0.5]$ of the original signal are processed separately. This can be obtained using either two decimation filters or a single lowpass filter and an adequate modulation of the original signal [31]. From a practical point of view, the latter is preferable because the useful spectral part always corresponds to the central half of the resulting subbands, *i.e.* $f \in [-0.25, 0.25]$. Thus, concerning the band $[0, 0.5]$, the decomposition is obtained starting with the signal:

$$x_0^{(0)}(n) := x(n)\exp(\imath\Omega n) \tag{14}$$

where $\Omega = -\pi/2$. This modulation will center the normalized frequency band $[0, 0.5]$ of $x(n)$ around 0. Figure 4b shows the effect of this operation on a synthetic signal. The decomposition from level ℓ to level $\ell + 1$ is then obtained as follows:

$$x_{\ell+1}^{(2i)}(n) = \sum_{n'} h(n')x_\ell^{(i)}(2n - n')e^{-\imath\Omega(2n-n')/2} \tag{15}$$

$$x_{\ell+1}^{(2i+1)}(n) = \sum_{n'} h(n')x_\ell^{(i)}(2n - n')e^{+\imath\Omega(2n-n')/2} \tag{16}$$

where $h(n)$ is a real lowpass filter with passband $[0, 0.125]$ and transition band $[0.125, f_{\max}]$, where $f_{max} \leqslant 0.25$ (lowpass filter in *Fig. 3b*). The spectra of the resulting signals are illustrated in Figure 4c at level $\ell = 1$. Each subsignal $x_\ell^{(i)}(n)$, where $i = 0, 1, \ldots, 2^\ell - 1$, has its useful spectrum in $[-0.25, 0.25]$. It is associated to the normalized frequency interval $[i/2^{\ell+1}, (i + 1)/2^{\ell+1}]$ of the original signal. The decomposition of the band $[-0.5, 0]$ is obtained in the same manner with $\Omega = +\pi/2$ in Equation (14) and using the same Equations (15, 16) to generate the subband signals. In this case, the resulting subsignals $x_\ell^{(i)}(n)$ correspond to the frequency interval $[-(i + 1)/2^{\ell+1}, -i/2^{\ell+1}]$.

The extension of this discussion for multidimensional signals is straightforward. For 2-D signals, the spectral bands $[-0.5, 0] \times [-0.5, 0]$, $[0, 0.5] \times [-0.5, 0]$, $[-0.5, 0] \times [0, 0.5]$ and $[0, 0.5] \times [0, 0.5]$ may be processed separately. Let $\Omega_1, \Omega_2 \in \{-\pi/2, +\pi/2\}$ be two modulation frequencies, then the four decomposition trees are obtained starting with:

$$x_0^{(0,0)}(n, m) := x(n, m)\exp(\imath\Omega_1 n + \imath\Omega_2 m) \tag{17}$$

and using the different combinations of Ω_1 and Ω_2. The decomposition from level ℓ to level $\ell + 1$ is obtained as follows:

$$x_{\ell+1}^{(2i+i',2j+j')}(n, m) = \sum_{n',m'} h(n', m')x_\ell^{(i,j)}(2n - n', 2m - m') \times e^{(-1)^{i'+1}\imath\Omega_1(2n-n')/2}e^{(-1)^{j'+1}\imath\Omega_2(2m-m')/2} \tag{18}$$

for $i', j' \in \{0, 1\}$. Here $h(n, m)$ is a unique 2-D lowpass filter having the same specifications as the 1-D filter discussed before for each dimension.

(4) This is also the reason why the measure of flatness in Equation (10) is computed only in the central part of the spectral domain.

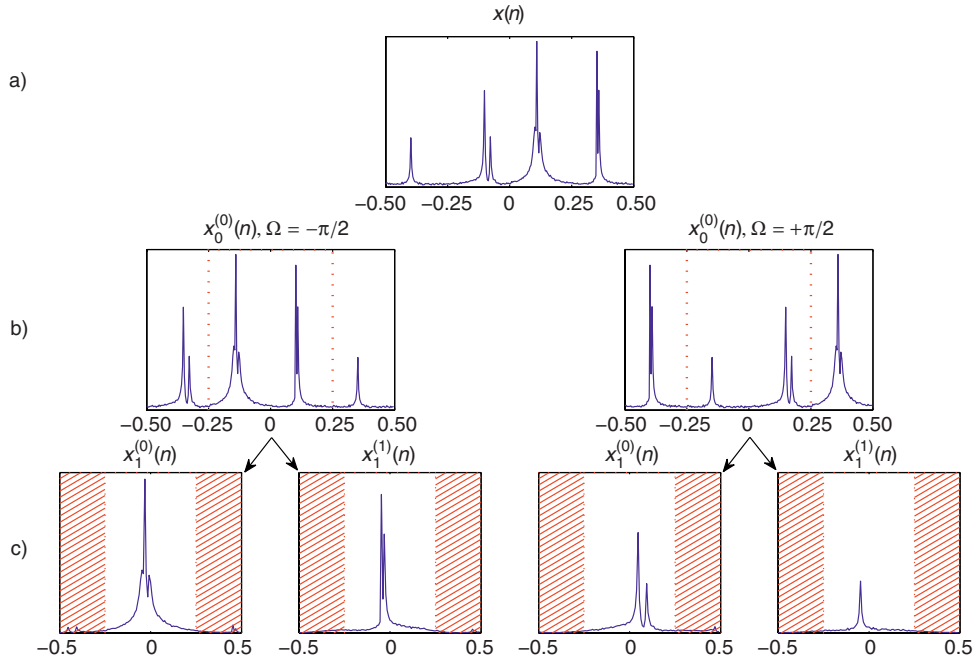

Figure 4

Spectral representation of the effect of modulation and filtering/decimation on a synthetic signal. a) Original signal; b) modulation with $\Omega = -\pi/2$ and $\Omega = +\pi/2$; c) filtering and downsampling. (...) Indication of the targeted frequency interval which is always $[-0.25, 0.25]$. Modes estimated in the dashed ranges must be discarded.

Once the subband signals are obtained, the corresponding parameters are estimated. Now these parameters have to be mapped to their fullband values. The conversion formulae are given in Appendix A for 1-D and 2-D signals.

3.2 The Free Parameters

A number of parameters have to be chosen by the user for this method to work. This is discussed in the present section.

At first, the user has to choose the estimation method. All spectral estimation methods may be used, especially those cited in the introduction. We have implemented several of them (LPSVD, HSVD, HOYWSVD [44], etc.) and we have observed that the results achieved are very close one to another. Generally, each method needs at least one parameter to be tuned. It is related to the dimension of the estimation model and is often called "prediction order". It depends strongly on the number of samples and components. The reader is referred to [39, 58] for more details on this topic. Also, a theoretical study of the estimation accuracy of eigenstructure-based model estimators has shown that an optimal prediction order is existing for damped complex exponential signals [59]. All estimation free-parameters are included in vector $\mathbf{p}$ in the algorithms presented in Tables 1, 2. Whatever the method used to estimate the signal parameters, it is indeed necessary to know the number of variables that have to be estimated, *i.e.* the number of modes. The latter is generally unknown, especially when considering subband signals. The solution to this problem is to use so-called order estimation criteria such as MDL and AIC [29, 60].

Concerning the decomposition scheme, three topics have to be discussed, namely the decimation filter, the maximum decimation depth $\ell_{\max}$ and the significance level α for the stopping rule:

- *the decimation filter.* A 1-D filter is generally designed using two parameters: the order and the cut-off frequency. These parameters can be obtained so as to meet some specifications in terms of passband and transition band widths and minimum attenuation in the stopband. In our case, the passband spreads from 0 to 0.125 and the transition band from 0.125 to 0.25. The attenuation of the filter is fixed between −40 and −60 dB so as to eliminate the out-of-band spectral lines. In order to obtain a 2-D filter, the easiest way is to design two 1-D filters, say $h_1(n)$ and $h_2(m)$, and compute the separable filter given by $h(n, m) = h_1(n)h_2(m)$;
- *the maximum decimation level.* The main constraint behind the choice of the value of $\ell_{\max}$ is the number of samples in deep nodes which must be not too low in order to preserve good estimation conditions. It is related to the length of the fullband signal but also to the general complexity of the signal;
- *the false alarm rate.* In the literature, it is generally set between 1 and 10%. From our experience, this parameter is far from being critical when chosen in the previous

interval since it influences little the final decimation level and not at all the estimation performances. In our simulations, we always use $\alpha = 1\%$.

TABLE 1

Algorithm for subband estimation of 1-D NMR

– **Input.** A 1-D signal $x(n) \in \mathbb{C}$, a low pass filter $h(n) \in \mathbb{R}$, a maximum decimation level $\ell_{\max}$, a false alarm rate α, and a set of estimation-related parameters $\mathbf{p}$.
– **Output.** Parameters $\hat{K}$ and $\{\hat{z}_k, \hat{a}_k\}_{k=1}^{\hat{K}}$.

1. **Initialize.** Set $x_0^{(0)}(n) = x(n)\exp(\imath\Omega n), \Omega = \pm\pi/2, \ell = 0$ and $i = 0$.
2. **Decompose.** Split $x_\ell^{(i)}(n)$ into two subbands $x_{\ell+1}^{(2i)}(n)$ and $x_{\ell+1}^{(2i+1)}(n)$, using Equations (15, 16).
3. **Estimate.** Find the subband parameters of the resulting signals:
$$[\hat{K}_{\ell+1}^{(2i+i')}, \hat{\mathbf{z}}_{\ell+1}^{(2i+i')}, \hat{\mathbf{a}}_{\ell+1}^{(2i+i')}] = \text{Estimate\_1D}\ (x_{\ell+1}^{(2i+i')}(n), \mathbf{p}) \quad \text{for } i' \in \{0, 1\}.$$
4. **Test.** Estimate the spectral flatness of the residuals in the two subbands using Equations (9) and (10), and mark each node as "decomposable" or "final".
5. **Iterate.** Find a decomposable node (ℓ, i) such that $\ell < \ell_{\max}$ in the whole tree and repeat 2-4. Exit if no node is decomposable.
6. **Output.** Return the fullband images of all subband parameters.

TABLE 2

Algorithm for subband estimation of 2-D NMR

– **Input.** A 2-D signal $x(n, m) \in \mathbb{C}$, a low pass filter $h(n, m) \in \mathbb{R}$, a maximum decimation level $\ell_{\max}$, a false alarm rate α, and a set of estimation-related parameters $\mathbf{p}$.
– **Output.** Parameters $\hat{K}$ and $\{\hat{z}_k, \hat{w}_k, \hat{a}_k\}_{k=1}^{\hat{K}}$.

1. **Initialize.** Set $x_0^{(0,0)}(n, m) = x(n, m)\exp(\imath\Omega_1 n + \imath\Omega_2 m), \Omega_{1,2} = \pm\pi/2, \ell = 0, i = 0$ and $j = 0$.
2. **Decompose.** Using Equation (18), split $x_\ell^{(i,j)}(n, m)$ into four subbands $x_{\ell+1}^{(2i+i',2j+j')}(n, m)$, where $i', j' \in \{0, 1\}$.
3. **Estimate.** Find the subband parameters of the resulting signals:
$$[\hat{K}_{\ell+1}^{(2i+i',2j+j')}, \hat{\mathbf{z}}_{\ell+1}^{(2i+i',2j+j')}, \hat{\mathbf{w}}_{\ell+1}^{(2i+i',2j+j')}, \hat{\mathbf{a}}_{\ell+1}^{(2i+i',2j+j')}] = \text{Estimate\_2D}\ (x_{\ell+1}^{(2i+i',2j+j')}(n, m), \mathbf{p}), \quad \text{for } i', j' \in \{0, 1\}.$$
4. **Test.** Estimate the spectral flatness of the residuals in the four subbands using Equations (13) and (10), and mark each node as "decomposable" or "final".
5. **Iterate.** Find a decomposable node (ℓ, i, j) such that $\ell < \ell_{\max}$ in the whole tree and repeat 2-4. Exit if no node is decomposable.
6. **Output.** Return the fullband images of all subband parameters.

TABLE 3

Chemical composition corresponding to the 1-D NMR signal

Products	Formulae	Quantity (g)
Toluene	C_7H_8	0.5322
Meta–ethyltoluene	C_9H_{12}	0.3395
Ethylbenzene	C_8H_{10}	0.3931
o-Xylene	C_8H_{10}	0.2986
1,3–Dimethyl–5–ethylbenzene	$C_{10}H_{14}$	0.2651
m-Xylene	C_8H_{10}	0.3089
Tetraline	$C_{10}H_{12}$	0.3312
Indane	C_9H_{10}	0.2893
n–Propylbenzene	C_9H_{12}	0.1593
p-Xylene	C_8H_{10}	0.1208
1,2–Dimethyl–3–ethylbenzene	$C_{10}H_{14}$	0.1150
1,3,5–Trimethylbenzene	C_9H_{12}	0.0806
Naphthalene	$C_{10}H_8$	0.0188
1,2,3–Trimethylbenzene	C_9H_{12}	0.0488
Isobuthylbenzene	$C_{10}H_{14}$	0.0132
Benzene	C_6H_6	0.0765
2,4–Dimethylhexane	C_8H_{18}	0.1012
2,3,4–Trimethylpentane	C_8H_{18}	0.1489
TMS	$C_4H_{12}Si$	–
Dioxane	$C_4H_8O_2$	–
Chloroform	$CDCl_3$	–

3.3 Summary of the Algorithms

The complete algorithms for processing 1-D and 2-D NMR data are summarized in Tables 1 and 2 respectively. It is worth noting that a MATLAB implementation of the 1-D algorithm, called SPENCER [5] for Subband Parameter Estimation of Noisy Complex Exponential data Records, is available for free download. It includes all the procedure presented here, including adaptive subband decomposition and parameter estimation. Moreover, it integrates other functionalities such as baseline suppression, phase correction, line listing and graphic representations. Similarly, a MATLAB implementation of the 2-D algorithm is also available from the authors.

4 EXPERIMENTAL RESULTS

4.1 1-D NMR

The signal, made up of 131 072 points, was recorded on a *Bruker* AM 400 spectrometer (^{13}C frequency observation: 100.62 MHz). It results from quantitative experiments on a synthesized mixture of nineteen compounds in $CDCl_3$, with TetraMethylSilane (TMS) as internal reference (see *Tab. 3*). Hence the complete chemical composition and the chemical shifts (δ/TMS) of the lines of the individual products are

(5) Download page: www.iris.cran.uhp-nancy.fr/spencer

TABLE 4

Results achieved in some subbands of the 1-D NMR signal. The first part on the left gives the theoretical lines with corresponding chemical component, chemical shifting (in ppm) and relative intensity (%) with respect to the toluene's line (25th line). The central part sets out the results of the FT+DCONV approach: estimated normalized frequencies, estimated relative intensities (directly calculated from estimated amplitudes). The right part reports the results achieved by the proposed subband method

Band		Theoretical			FT+DCONV		Proposed	
(ℓ, i)	Line	component	δ (ppm)	A (%)	f	A (%)	f	A (%)
⋮	⋮	⋮	⋮	⋮	⋮	⋮	⋮	⋮
	23	iso-BuBenzene	129.13	1.70	–	–	–	–
	24	Tetraline	129.11	43.37	0.14073	42.02	0.14072	40.20
(8, 72)	25	Toluene	129.06	100.00	0.14092	100.00	0.14092	100.00
	26	*p*-Xylene	128.94	39.40	0.14124	40.16	0.14124	41.30
	27	*m*-EtToluene	128.72	24.45	0.14181	25.25	0.14181	25.60
	28	*n*-PrBenzene	128.47	22.98	0.14239	21.27	0.14239	23.96
	29	Benzene	128.37	50.86	0.14267	51.20	0.14266	51.48
	30	EthylBenzene	128.31	64.11	0.14275	66.86	0.14275	61.31
	31	Toluene	128.25	100.00	0.14293	65.22	0.14293	82.66
	32	*n*-PrBenzene	128.23	22.98	0.14297	75.81	0.14297	43.04
(8, 73)	33	*m*-EtToluene	128.23	24.45	0.14301	12.94	0.14301	35.55
	34	*m*-Xylene	128.15	25.19	0.14315	23.62	0.14315	25.10
	35	iso-BuBenzene	128.07	1.70	–	–	–	–
	36	Naphthalene	127.88	5.08	0.14382	8.24	0.14382	6.13
	37	EthylBenzene	127.86	64.11	0.14392	64.67	0.14392	63.04
⋮	⋮	⋮	⋮	⋮	⋮	⋮	⋮	⋮
							0.27024	13.06
	58	$CDCl_3$	77.30		0.27064	1 923.5	0.27063	1 955.1
							0.27077	39.98
(7, 69)	59	$CDCl_3$	77.00		0.27143	1 914.9	0.27143	1 987.7
							0.27173	26.96
	60	$CDCl_3$	76.70		0.27223	1 961.9	0.27223	1 934.1
							0.27232	44.36
⋮	⋮	⋮	⋮	⋮	⋮	⋮	⋮	⋮
	70	2,3,4-triMePentane	29.67	21.45	0.39087	23.72	0.39088	20.94
	71	Tetraline	29.37	43.37	0.39158	38.83	0.39158	42.97
(6, 50)	72	EthylBenzene	28.89	32.05	0.39283	34.18	0.39282	36.42
	73	*m*-EtToluene	28.85	24.45	0.39303	27.02	0.39303	26.71
	74	1,3-diMe-5-EtBenzene	28.72	17.10	0.39326	19.20	0.39326	18.59
	75	1,2-diMe-3-EtBenzene	26.98	7.42	0.39765	9.85	0.39764	8.94
⋮	⋮	⋮	⋮	⋮	⋮	⋮	⋮	⋮
	83	2,3,4-triMePentane	21.75	21.45	0.41079	20.32	0.41079	21.15
	84	Toluene	21.46	50.00	0.41151	48.17	0.41151	46.82
(8, 210)	85	*m*-EtToluene	21.41	24.45	0.41164	21.10	0.41164	20.58
	86	*m*-Xylene	21.33	50.38	0.41182	49.78	0.41182	48.28
	87	1,3-diMe-5-EtBenzene	21.27	34.20	0.41197	37.97	0.41197	33.25
	88	1,3,5-triMeBenzene	21.20	17.42	0.41215	17.68	0.41215	15.92
(8, 211)	89	*p*-Xylene	20.99	19.70	0.41278	20.07	0.41278	21.12
	90	1,2-diMe-3-EtBenzene	20.67	7.42	0.41351	5.89	0.41350	7.09
	91	1,2,3-triMeBenzene	20.54	7.03	0.41382	5.38	0.41382	5.98
⋮	⋮	⋮	⋮	⋮	⋮	⋮	⋮	⋮

known. Some of them are shown in Table 4. Toluene being the most concentrated compound, two lines (25 and 31) have the maximum intensity. The latter is therefore set to 100% and, from the theoretical composition, the intensities of the other lines are expressed as a percentage of these reference lines.

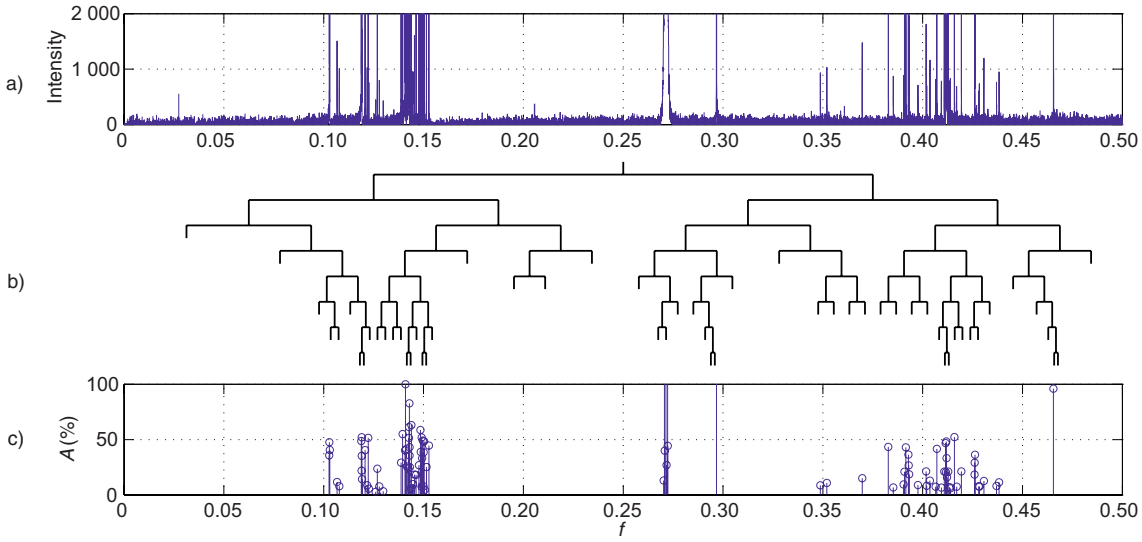

Figure 5

a) spectrum of the 1-D NMR signal, b) decomposition tree, c) resulting line listing.

The decimation FIR (Finite Impulse Response) filter was designed with an equiripple routine using $f_{\max} = 0.25$, an attenuation of −60 dB and a passband ripple of about 0.1 dB. The maximum decomposition level is set to $\ell_{\max} = 8$. Concerning the estimation method, we have tried several of them and the results achieved are very close. We present here those given by LPSVD [13] with parameter $p = 60$. The Adaptive SubBand (ASB) decomposition associated to LPSVD will be called ASB-LPSVD. The results are compared to those given by a classical method which associates a classical FT approach with a maximum likelihood deconvolution algorithm (FT+DCONV) [10, 61]. The latter is used in the best possible conditions, that is it makes use of the entire signal and, during the deconvolution process, the exact number of components K (which is perfectly known, $K = 104$) is used. Hence, the FT+DCONV algorithm is considered as the reference method for this signal. Note that K being known, the use of adapted thresholds allowed us to insist on the presence of some lines and to eliminate all supplementary ones, which is generally not possible in practice.

The decomposition achieved by ASB-LPSVD is represented in Figure 5. As expected, it can be seen that the decomposition is carried on relatively to the complexity of the subbands encountered. Hence the decomposition is deeper where a lot of lines are present and/or they are hard to estimate. For instance, the band $(3, 0)$, *i.e.* obtained at level $\ell = 3$ and with frequency shift $i = 0$, depicted in Figure 6 corresponds to a case where the decomposition was stopped at an early stage. This is because it does not contain any significant line except an artifact around frequency

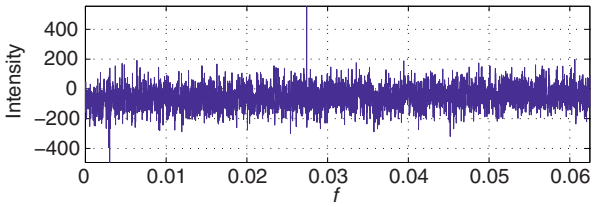

Figure 6

Example of "empty band" in the 1-D NMR signal: subband $(3, 0)$.

0.028. The latter was rightly not detected because it does not figure a damped mode. Globally, the ASB-LPSVD method detects 100 lines among which 94 correspond to actual theoretical composition, and 6 "extra-lines" seems to have no theoretical correspondent. Thus ten theoretical lines are not detected. FT+DCONV made only 93 good detections and missed 11 theoretical lines, despite of the use of the correct number of modes. The results are partly presented in Table 4 together with the theoretical line spectrum.

Concerning the 10 lines not retrieved by the subband approach, two different situations may be distinguished: non-detection of peaks with very small amplitudes (<2%), and non-separation of 2 lines. In the first case, the products involved are in very small quantities, and the corresponding peaks are almost invisible in the FT absorption spectrum (that is the case, for example, for lines 23 and 35). In the second case, two different products have almost the same

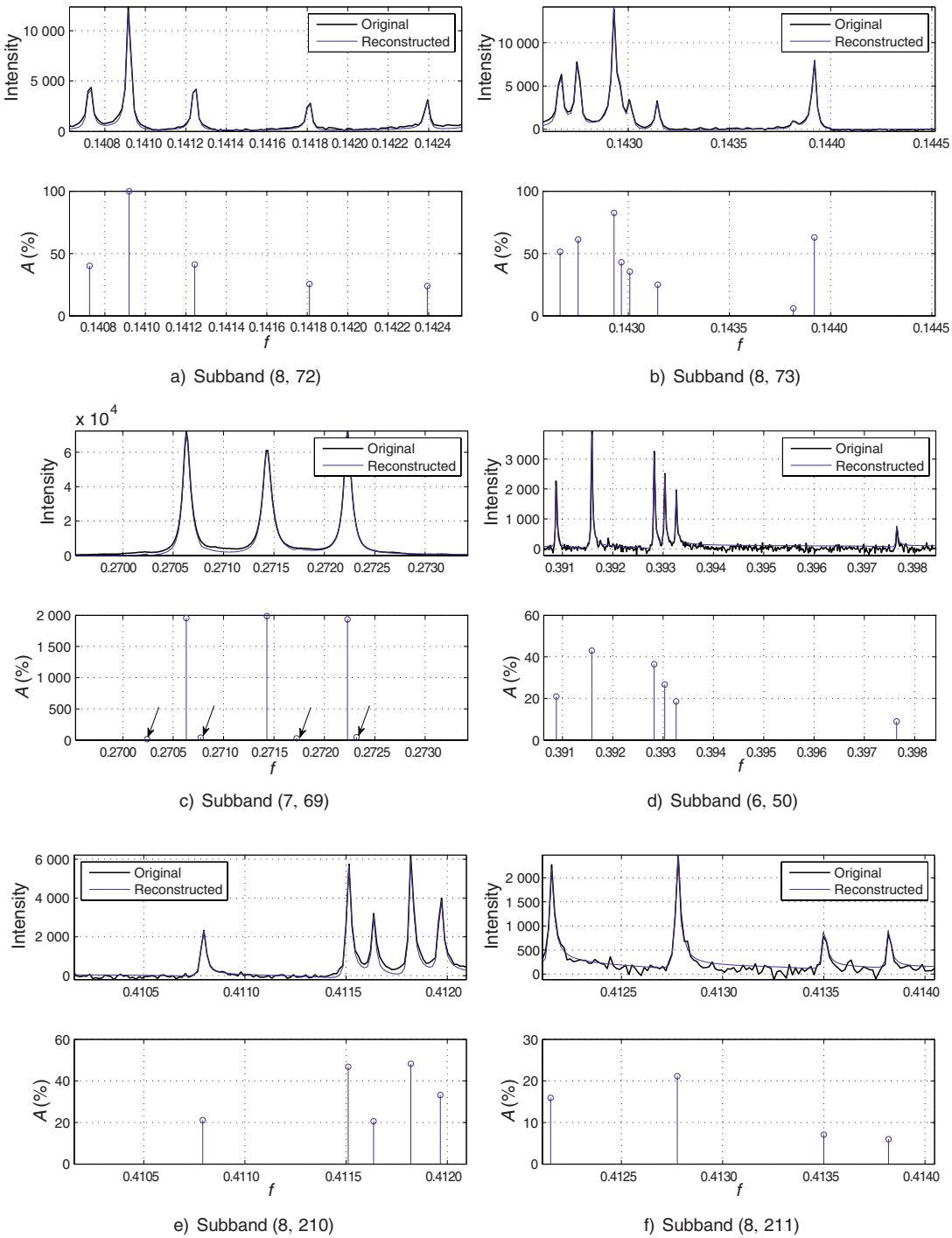

Figure 7

Details obtained in some subbands of the 1-D NMR signal. Arrows point out spurious peaks.

resonance frequency (0.10286 and 0.10288) and thus could not be separated by any method.

Concerning the 6 extra-lines, two different cases may be distinguished. In the first case, the algorithm tends to fit two different lines in place of a broad one. For example, this can be observed in band (7, 69) (*Tab. 4*, *Fig. 7*) which shows 4 false lines estimated close to the resonant frequencies of the solvant. In fact, this is caused by a bad estimation of the number of peaks and this kind of phenomenon often occurs in the vicinity of peaks with strong intensities. In the second case, some extra-lines may correspond to impurities in the mixture considered. In any case, all extra-lines have

generally very small amplitudes relatively to the neighbor lines and may be eliminated by simple thresholding adapted to the subband at hand.

Some subbands of interest obtained with ASB-LPSVD are depicted in Figure 7. Each subfigure shows the FT absorption spectrum together with the estimated line spectrum. It can be seen that there is a good correspondence between the estimated lines and the signal spectrum. It is worth noting that the subbands have different widths because they were obtained at different levels, depending on their complexity. Indeed, the algorithm may detect correctly all modes and thus stop the decomposition before the maximum level is attained, *e.g.* as in band (6, 50) in Figure 7d.

Generally speaking, note that the precision of frequency estimates is quite irreproachable. Concerning more particularly amplitude estimation, the mean relative errors observed with the two methods are comparable. Note the important errors made by the deconvolution method in the case of lines 31, 32 and 33, when the ASB-LPSVD method keeps a more reasonable behaviour.

4.2 2-D NMR

We consider an experimental 2-D NMR signal of size 64×2048. The 2-D decimation filter is separable into two 1-D filters which are the same as in the 1-D case (ripple amplitude 0.1 dB, stopband attenuation −60 dB). Since the NMR data set has a large amount of samples in the second dimension, we fixed the minimum decimation level (without estimation) to $\ell_{\min} = [\![1; 2]\!]$ and the maximum one to $\ell_{\max} = [\![2; 4]\!]$. The notation $[\![x; y]\!]$ stands for column vectors, with x and y corresponding to the first and second dimension, respectively. We used the TLS-Prony method [24] with prediction orders set to $\mathbf{p} = [\![N'/2; M'/2]\!]$, where $N' \times M'$ is the size of the subband signal.

The final subbands obtained with our algorithm in the spectral region $[-0.25, 0] \times [-0.25, -0.25]$ are shown in Figure 8. As it was the case in 1-D, one can observe that the decomposition is generally deeper in the spectral regions where several modes are located. On the other hand, for remote modes, the decomposition is stopped at an early level. This is the case for instance with the mode located in the band $[-0.250, -0.125] \times [-0.0625, 0]$. So here again the method is able to adapt itself to the local complexity of a signal, allowing one to reduce the calculation time, as compared to a uniform decomposition in which several small subbands need to be analysed. The results obtained in some subbands are represented in Figure 9, where the estimated modes are indicated with thick circles. For the subband in Figure 9a, 13 modes have been detected among which 10 correspond to true peaks. We observe also in Figure 9b that the approach tend to fit a very large peak by several small ones. Finally, some very close modes have been resolved as illustrated in Figures 9c,d.

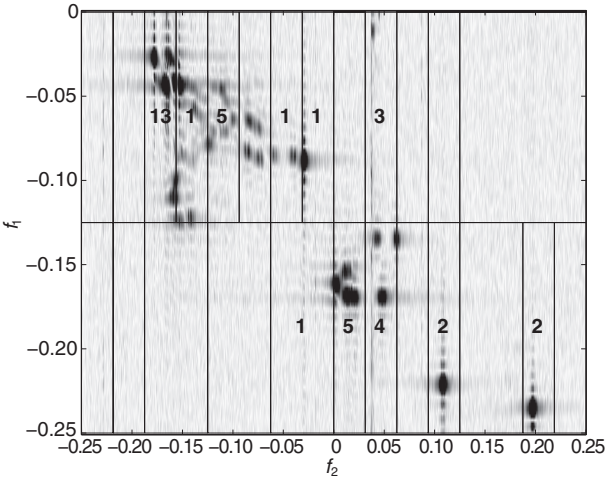

Figure 8

Spectral region $[-0.25, 0] \times [-0.25, -0.25]$ of the 2-D NMR signal with the final subbands and the number of estimated modes.

CONCLUSION

Subband decomposition is known to have several advantages in terms of detection rate, frequency resolution, and numerical complexity relatively to fullband estimators. Moreover, this technique is able to handle with signals of high complexity (*i.e.* long NMR signals with many modes). The adaptive scheme proposed in the present paper, further improves the performances of the subband decomposition in the sense that there is no more need to select the decimation depth. Indeed, the method automatically selects the signal-bearing bands and decides whether or not a band should be further decomposed. The adaptive subband decomposition uses a stopping rule based on the spectral flatness of the subband residuals: the decomposition is stopped on a given subband only if the residuals are close to white noise. The advantage of such a criterion is its ability to detect some missed modes and to ensure that the parameters are correctly estimated. More generally, this approach allows one to avoid a manual selection of the frequency intervals in which the estimation process is performed, as it would be the case with classical subband methods.

The effectiveness of the proposed method is demonstrated using real-world 1-D and 2-D NMR signals. When dealing with intricate 1-D spectra, the results show that it performs at least comparably to a classical FT+DCONV procedure in terms of frequency and amplitude estimates. But recall that, in practice, the deconvolution procedure requires a prior determination of the number of peaks. Here, the FT+DCONV algorithm was used with the assumption of a perfectly known number of components. On the contrary, our approach is single-step, neither deconvolution nor

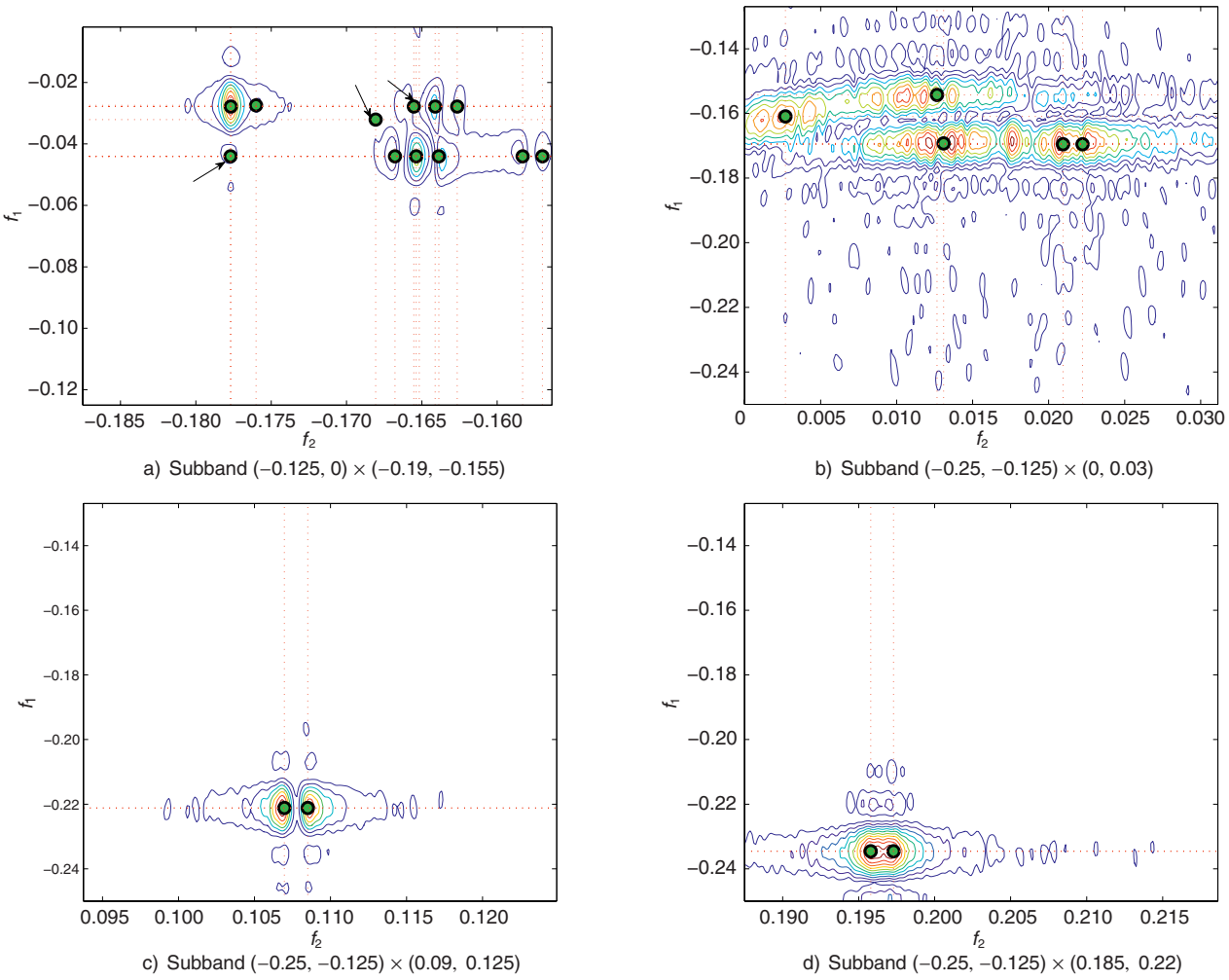

Figure 9

Reconstructed contour plot in some subbands of the 2-D NMR signal. (●) Position of the estimated modes. (...) coordinates of the modes. Arrows point out spurious peaks.

numerical integration is necessary and the parameters are given directly with moderate computation times. It is about 10 seconds on a standard PC for 1-D signals containing a hundred modes and made up of 128k samples (as compared to several minutes for FT+DCONV). In addition, its resolution capabilities are superior, thus it is able to increase the number of correctly detected lines.

It is worth mentionning that the resulting adaptive subband decomposition can be seen as a hierarchical oversampled filter banks, implemented as packets. In that respect, following [62], the proposed approach corresponds to an adaptive tree structured processing in which each subband can be seen as a dictionary element. In 2-D NMR application, possible extensions of the proposed approach may consist in the use of more adapted representation, using dictionary elements, better accounting for the potential anisotropy or obliquity of the 2-D NMR data.

Finally, the proposed decomposition is presented under the Lorentzian shape assumption and the experimental results were achieved using eigenanalysis-based methods. Indeed, the proposed scheme may also be applied with other lineshape models and/or any estimation algorithm.

REFERENCES

1 Cavanagh J., Fairbrother W.J., Palmer A.G., Skelton N.J., Rance M. (2006) *Protein NMR Spectroscopy: Principles and Practice*, Academic Press, San Diego, CA.

2 Bax A. (1985) A simple description of two-dimensional NMR spectroscopy, *Bull. Magn. Reson.* **7**, 4, 167-183.

3 Bax A., Lerner L. (1986) Two-dimensional nuclear magnetic resonance spectroscopy, *Science* **232**, 960-967.

4 Canet D. (1996) *Nuclear magnetic resonance spectroscopy. Concepts and methods*, John Wiley & Sons Ltd, West Sussex, England.

5 Marshall I., Bruce S.D., Higinbotham J., MacLullich A., Wardlaw J.M., Ferguson K.J., Seckl J. (2000) Choice of spectroscopic lineshape model affects metabolite peak areas and area ratios, *Magn. Reson. Med.* **44**, 646-649.

6 Suvichakorn A., Antoine J.P. (2008) Analyzing NMR spectra with the Morlet wavelet, *Proc. 16th European Signal Process. Conf. EUSIPCO 2008*, Lausanne, Suisse, 25-29 Aug.

7 Bartha R., Drost D.J., Menon R.S., Williamson P.C. (2000) Spectroscopic lineshape correction by QUECC: Combined QUALITY deconvolution and eddy current correction, *Magn. Reson. Med.* **44**, 641-645.

8 Marple S.L. (1987) *Digital spectral analysis with applications*, Prentice Hall, Englewood Cliffs.

9 Kay S.M. (1988) *Modern spectral estimation. Theory and application*, Prentice Hall, Englewood Cliffs.

10 Matlengiewicz M., Henzel N., Czachowska D., Schmit-Quilès F., Nicole D., Lauer J.C. (1994) Computer aided analysis of ^{13}C NMR spectra of multicomponent mixtures: 3. Analysis of individual components of a heavy gasoline from liquefaction of Polish coal, *Fuel* **73**, 6, 843-850. ISSN 0016-2361.

11 Bresler Y., Macovski A. (1986) Exact maximum likelihood parameter estimation of superimposed exponential signals in noise, *IEEE Trans. Acoust. Speech Signal Process.* **34**, 5, 1081-1089.

12 Rubtsov D.V., Griffin J.L. (2007) Time-domain Bayesian detection and estimation of noisy damped sinusoidal signals applied to NMR spectroscopy, *J. Magn. Reson.* **188**, 367-379.

13 Kumaresan R., Tufts D.W. (1982) Estimating the parameters of exponentially damped sinusoids and pole-zero modeling in noise, *IEEE Trans. Acoust. Speech Signal Process.* **30**, 833-840.

14 Kung R., Arun K.S., Bhaskar Rao D.V. (1983) State-space and singular value decomposition-based approximation methods for the harmonic retrieval problem, *J. Opt. Soc. Am.* **73**, 12, 1799-1811.

15 Hua Y., Sarkar T.K. (1990) Matrix pencil method for estimating parameters of exponentially damped/undamped sinusoids in noise, *IEEE Trans. Acoust. Speech Signal Process.* **38**, 5, 814-824.

16 Barkhuijsen H., de Beer R., Bovée W.M.M.J, van Ormondt D. (1985) Retrieval of frequencies, amplitudes, damping factors, and phases from time-domain signals using a linear least-squares procedure, *J. Magn. Reson.* **63**, 465-481.

17 Barkhuijsen H., de Beer R., van Ormondt D. (1987) Improved algorithm for noniterative time domain model fitting to exponentially damped magnetic resonance signals, *J. Magn. Reson.* **73**, 553-557.

18 Hoch J.C., Stern A.S. (1996) *NMR data processing*, Wiley-Liss, New York.

19 Koehl P. (1999) Linear prediction spectral analysis of NMR data, *Prog. NMR Spectr.* **34**, 257-299.

20 Van Huffel S., Chen H., Decaniere C., Van Hecke P. (1994) Algorithm for time-domain NMR data fitting based on total least squares, *J. Magn. Reson. Ser. A* **110**, 228-237.

21 Poullet J.B., Sima D.M., Van Huffel S. (2008) MRS signal quantitation: A review of time- and frequency-domain methods, *J. Magn. Reson.* **195**, 134-144.

22 Clark M.P., Scharf L.L. (1994) Two-dimensional modal analysis based on maximum likelihood, *IEEE Trans. Signal Process.* **42**, 6, 1443-1452.

23 Li Y., Razavilar J., Ray K.J. (1998) A high-resolution technique for multidimensional NMR spectroscopy, *IEEE Trans. Biomed. Eng.* **45**, 1, 78-86.

24 Sacchini J.J., Steedly W.M., Moses R.L. (1993) Two-dimensional Prony modeling and parameter estimation, *IEEE Trans. Signal Process.* **41**, 11, 3127-3137.

25 Hua Y. (1992) Estimating two-dimensional frequencies by matrix enhancement and Matrix Pencil, *IEEE Trans. Signal Process.* **40**, 9, 2267-2280.

26 Liu X., Sidiropoulos N. (2002) On constant modulus multidimensional harmonic retrieval, *Proc. IEEE ICASSP 2002*, Orlando, Florida, 13-17 May, Vol. 3, pp. 2977-2980.

27 Sidiropoulos N.D. (2001) A new 2-D harmonic retrieval algorithm, *Proc. 39th Allerton Conf. Comm. Control Computing*, Urbana-Champaign, October.

28 Rouquette S., Najim M. (2001) Estimation of frequencies and damping factors by two-dimensional ESPRIT type methods, *IEEE Trans. Signal Process.* **49**, 1, 237-245.

29 Wax M., Kailath T. (1985) Detection of signals by information theoretic criteria, *IEEE Trans. Acoust. Speech Signal Process.* **33**, 2, 387-392.

30 Sandgren N., Stoica P., Frigo F.J. (2006) Area selective signal parameter estimation for two-dimensional MR spectroscopy data, *J. Magn. Reson.* **183**, 50-59.

31 Silverstein S.D., Engeler W.E., Tardif J.A. (1991) Parallel architectures for multirate superresolution spectrum analyzers, *IEEE Trans. Circ. Syst.* **38**, 4, 449-453.

32 Steedly W.M., Ying C.-H.J., Moses R.L. (1994) A modified TLS-Prony method using data decimation, *IEEE Trans. Signal Process.* **42**, 9, 2292-2303.

33 Tkacenko A., Vaidyanathan P.P. (2001) The role of filter banks in sinusoidal frequency estimation, *J. Franklin Inst.* **338**, 5, 517-547.

34 Zoltowski M.D., Kautz G.M., Silverstein S.D. (1993) Beamspace Root-MUSIC, *IEEE Trans. Signal Process.* **41**, 1, 344-364.

35 Tang J., Norris J.R. (1988) LP-ZOOM, a linear prediction method for local spectral analysis of NMR signals, *J. Magn. Reson.* **79**, 190-196.

36 Mandelshtam V.A. (2001) FDM: the filter diagonalization method for data processing in NMR experiments, *Prog. NMR Spectr.* **38**, 159-196.

37 Rao S., Pearlman W. (1996) Analysis of linear prediction, coding, and spectral estimation from subbands, *IEEE Trans. Inf. Theory* **42**, 4, 1160-1178.

38 Stoica P., Nordsjö A.E. (1997) Subspace-based frequency estimation in the presence of moving-average noise using decimation, *Signal Process.* **63**, 211-220.

39 Djermoune E.-H., Tomczak M., Mutzenhardt P. (2004) An adaptive subband decomposition approach for automatic analysis of NMR data, *J. Magn. Reson.* **169**, 1, 73-84.

40 Dologlou I., Van Huffel S., van Ormondt D. (1998) Frequency-selective MRS data quantification with frequency prior knowledge, *J. Magn. Reson.* **130**, 2, 238-243.

41 Mandelshtam V.A., Taylor H.S., Shaka A.J. (1998) Application of the filter diagonalization method to one- and two-dimensional NMR spectra, *J. Magn. Reson.* **133**, 304-312.

42 Romano R., Motta A., Camassa S., Pagano C., Santini M.T., Indovina P.L. (2002) A new time-domain frequency-selective quantification algorithm, *J. Magn. Reson.* **155**, 2, 226-235.

43 Stoica P., Sandgren N., Selén Y., Vanhamme L., Van Huffel S. (2003) Frequency-domain method based on the singular value decomposition for frequency-selective NMR spectroscopy, *J. Magn. Reson.* **165**, 1, 80-88.

44 Tomczak M., Djermoune E.-H. (2002) A subband ARMA modeling approach to high-resolution NMR spectroscopy, *J. Magn. Reson.* **158**, 86-98.

45 Vanhamme L., Sundin T., Van Hecke P., Van Huffel S., Pintelon R. (2000) Frequency-selective quantification of biomedical magnetic resonance spectroscopy data, *J. Magn. Reson.* **143**, 1, 1-16.

46 Sandgren N., Selén Y., Stoica P., Li J. (2004) Parametric methods for frequency-selective MR spectroscopy, *J. Magn. Reson.* **168**, 259-272.

47 Coifman R.R., Wickerhauser M.V. (1992) Entropy-based algorithms for best basis selection, *IEEE Trans. Inf. Theory* **38**, 2, 713-718.

48 Donoho D.L., Johnstone I.M. (1994) Ideal denoising in an orthonormal basis chosen from a library of bases. Technical Report 461, Dept. of Statistics, Stanford University, Sept.

49 Meyer F.G., Averbuch A., Strömberg J.-O. (2000) Fast adaptive wavelet packet image compression. *IEEE Trans. Image Process.* **9**, 5, 792-800.

50 Moulin P. (1996) Signal estimation using adapted tree-structured bases and the MDL principle, *IEEE Int. Symp. Time-Frequency and Time-Scale Analysis*, Paris, 18-21 June, pp. 141-143.

51 Mainardi L.T., Origgi D., Lucia P., Scotti G., Cerutti S. (2002) A wavelet packets decomposition algorithm for quantification of *in vivo* ^{1}H-MRS parameters, *Med. Eng. Phys.* **24**, 201-208.

52 van den Branden Lambrecht C., Karrakchou M. (1995) Wavelet packet-based high-resolution spectral estimation, *Signal Process.* **47**, 135-144.

53 Tomczak M., Djermoune E.-H., Mutzenhardt P. (2007) High-resolution MR spectroscopy *via* adaptive sub-band decomposition, Castleman B.C. (ed.), *New Research on Magnetic Resonance Imaging*, Novascience Publishers, Chap. 9, pp. 241-289.

54 Priestley M.B. (1989) *Spectral analysis and time series*, Academic Press, San Diego, CA.

55 Drouiche K. (2000) A new test for whiteness, *IEEE Trans. Signal Process.* **48**, 7, 1864-1871.

56 Djermoune E.-H. (2003) Estimation des paramètres de sinusoïdes amorties par décomposition en sous-bandes adaptative. Application à la spectroscopie RMN, *PhD thesis*, Université Henri Poincaré, Nancy 1, France.

57 Djermoune E.-H., Tomczak M. (2004) An adapted filterbank for frequency estimation, *Proc. 12th European Signal Image Process. Conf. EUSIPCO 2004*, Vienna, Austria, 6-10 Sept., pp. 2171-2174.

58 Djermoune E.-H., Brie D., Tomczak M. (2009) A subband algorithm for estimating the parameters of two-dimensional exponential signals, *Proc. European Signal Process. Conf., EUSIPCO 2004*, Glasgow, Scotland, 25-28 Aug.

59 Djermoune E.-H., Tomczak M. (2009) Perturbation analysis of subspace-based methods in estimating a damped complex exponential, *IEEE Trans. Signal Process.* **57**, 11, 4558-4563.

60 Reddy V.U., Biradar L.S. (1993) SVD-based information theoretic criteria for detection of the number of damped/undamped sinusoids and their performance analysis, *IEEE Trans. Signal Process.* **41**, 2872-2881.

61 Denoyer L.K., Dodd J.G. (1991) Maximum likelihood deconvolution for spectroscopy and chromatography, *Amer. Lab.* **23**, 19-22.

62 Jacques L., Duval L., Chaux C., Peyré G. (2011) A panorama on multiscale geometric representations, intertwining spatial, directional and frequency selectivity, *Signal Process.* **91**, 12, 2699-2730.

Final manuscript received in October 2012
Published online in March 2013

APPENDIX
FULLBAND IMAGES OF SUBBAND PARAMETERS

For 1-D signals, suppose that the modes estimated at node (ℓ, i) are denoted $\hat{z}'_k$. Then, the corresponding fullband modes can be found as follows [39]:

$$\hat{z}_k = \hat{z}'^{\,1/2^\ell}_k \exp\left(\imath\pi\frac{2i+1}{2^{\ell+1}}\right), \qquad \text{for band } [0, 0.5] \tag{A.1}$$

$$\hat{z}_k = -\hat{z}'^{\,1/2^\ell}_k \exp\left(\imath\pi\frac{2i+1}{2^{\ell+1}}\right), \qquad \text{for band } [-0.5, 0] \tag{A.2}$$

Similarly, for 2-D signals, the fullband images of subband modes $(\hat{z}'_k, \hat{w}'_k)$ at node (ℓ, i, j) are:

$$\hat{z}_k = (-1)^{i'} \hat{z}'^{\,1/2^\ell}_k \exp\left(\imath\pi\frac{2i+1}{2^{\ell+1}}\right) \tag{A.3}$$

$$\hat{w}_k = (-1)^{j'} \hat{w}'^{\,1/2^\ell}_k \exp\left(\imath\pi\frac{2j+1}{2^{\ell+1}}\right) \tag{A.4}$$

for band $[-0.5i', 0.5(1-i')]\times[-0.5j', 0.5(1-j')]$, where $i', j' \in \{0, 1\}$. The amplitudes may also be transformed from subband to fullband (see [39]). But, since the calculation of amplitudes is a linear problem when the fullband modes are computed, it is also possible to get their estimates directly from the fullband signal.